

This manuscript has been submitted for publication in **Computers & Geosciences**. The paper has not yet undergone peer-review. Subsequent versions of this manuscript may have slightly different content. If accepted, the final version of this manuscript will be available via the 'Peer-reviewed Publication DOI' link on the right-hand side of this webpage. Please feel free to contact any of the authors; we welcome feedback.

Fault Representation in Structural Modelling with Implicit Neural Representations

Kaifeng Gao^{a,*}, Florian Wellmann^{a,b}

^a*Institute of Computational Geoscience, Geothermics and Reservoir Geophysics (CG3), RWTH Aachen University, Aachen, 52074, Germany*

^b*Fraunhofer Research Institution for Energy Infrastructures and Geothermal Systems (IEG), Aachen, 52062, Germany*

ARTICLE INFO

Keywords:

Structural geology
Implicit geological modelling
Faults
Neural networks
Implicit neural representations

ABSTRACT


Implicit neural representations have been demonstrated to provide a flexible and scalable framework for computer graphics and three-dimensional modelling and, consequently, have found their way also into geological modelling. These networks are feature-based and resolution-independent, making them effective for modelling geological structures from scattered interface points, units, and structural orientations. Despite the promising characteristics of existing implicit neural representation approaches, modelling faults within implicit neural representations remains a significant challenge. In this work, we present a fault feature encoding approach to represent faults in implicit neural representations, where the discontinuous information is concatenated as additional features of observation points and query points for network input. We apply this methodology first to a synthetic model to evaluate its efficacy, and subsequently to a real-world dataset from a part of the Gullfaks field in the northern North Sea. The modelling results demonstrate the method's capacity to generate a well-defined implicit scalar field while preserving sharp transitions at fault locations. Moreover, this work mentions the advantages of the presented approach over using Boolean operations and discontinuous activation functions. Furthermore, we discuss the potential opportunity to integrate prior domain knowledge and geophysics datasets into structural modelling by embedding them as model input features or incorporating them as constraints by loss functions.

CRedit authorship contribution statement

Kaifeng Gao: Conceptualization, Investigation, Methodology, Software, Validation, Visualization, Writing - original draft, Writing - review & editing. **Florian Wellmann:** Conceptualization, Supervision, Resources, Writing - review & editing.

1. Introduction

To develop underground reservoirs sustainably and reliably, a critical issue is a thorough understanding of subsurface geometry, as it directly influences resource extraction, risk management, and reservoir development strategies. The importance of geometry in the understanding and simulation of geological processes has been well demonstrated (e.g., Wellmann and Caumon, 2018). A three-dimensional structural model serves as a powerful tool for representing subsurface geometry, integrating various constraints such as outcrop observations, interfaces, orientations, and geological units, thereby facilitating a more comprehensive understanding of the underground environment. Moreover, the appropriate methodology employed in developing a three-dimensional structural model must consider not only the geological complexity and the availability of data but also the required accuracy and model scale to ensure the model's reliability (Calcagno et al., 2008; Pyrcz and Deutsch, 2014; Ringrose and Bentley, 2015).

 kai.feng.gao@cg3.rwth-aachen.de (K. Gao)

ORCID(s): 0000-0003-0181-6602 (K. Gao); 0000-0003-2552-1876 (F. Wellmann)

The commonly used three-dimensional structural modelling approaches can be separated into explicit and implicit representations of the modelled geometry. We refer to Wellmann and Caumon (2018) for a detailed description of the general approaches and implementations. In implicit modelling, the modelling objective is to generate a continuous scalar field in such a way that an iso-surface of this field represents a relevant geological structure. The iso-surfaces corresponding to structural interfaces are extracted as the modelled geological structures, while discontinuities can be represented by scalar value jumps. The typical implicit modelling approaches are co-kriging interpolation (Calcagno et al., 2008; Lajaunie et al., 1997; de la Varga et al., 2019), radial basis function interpolation (Hillier et al., 2014; Carr et al., 2001), and discrete smooth interpolation (Grose et al., 2021b; Mallet, 1992, 1997). Recently, Gaussian processes, a machine learning approach, have been applied to geomodelling in both regression (Gonçalves et al., 2022) and classification scenarios (Gonçalves et al., 2017, 2023). While these methods demonstrate many promising characteristics, modelling large-scale and high-dimensional datasets remains challenging. This difficulty arises because these interpolation techniques require solving a linear matrix system to compute undetermined parameters, which is a time-consuming process when dealing with massive numbers of interpolation points, and the computational complexity limits its ability in high-dimensional data.

In recent years, there has been increasing interest in applying neural network techniques to geomodelling, including approaches such as Graph Neural Networks (GNN) (Hillier et al., 2021), Convolutional Neural Networks (CNN) (Bi et al., 2022), and Multilayer Perceptron (MLP) (Guo et al., 2024; Hillier et al., 2023). The core concept behind these methods is the use of neural networks to parameterize implicit functions that define the geometry and properties of geological models. By describing the relationships between geological observations (such as interface points, orientations, and rock types) and geological structures (such as interfaces, faults, and unconformities), these approaches can generate accurate and smooth geological models capable of both interpolation and extrapolation beyond the observed data.

Neural Network Geomodelling (NNG) approaches represent a progress from model-driven modelling to data-driven modelling. Traditional implicit geomodelling methods, such as kriging or radial basis functions, typically involve adapting constraint points to fit a known functional form, necessitating an evaluation of the impact of these forms on the modelling process. In contrast, NNG approaches are data-driven approaches in which coordinates and other prior knowledge are parameterized as model input features. Instead of generating a function that parameterizes the geological model as a mathematical formula, NNG approaches represent the model through a set of learnable neural network parameters.

One significant advantage of NNG approaches in geological modelling is their ability to efficiently handle large-scale and high-dimensional datasets. The advancement of fundamental neural network theory, along with the development of advanced optimization techniques and the implementation of parallel computing via frameworks such as TensorFlow

and PyTorch, has significantly reduced the computational burden associated with traditional methods (Hillier et al., 2023). This makes NNG approaches particularly well-suited for processing large-scale data in geomodelling. Moreover, traditional geomodelling methods often face challenges in integrating diverse datasets and geological knowledge into the modelling process. In contrast, NNG methods are feature-based, resolution-independent, and purely data-driven, providing a flexible and scalable framework for the integration of various forms of geological data and prior knowledge. As long as the geological data and knowledge can be represented as appropriate features or incorporated through a properly designed loss function to constrain the difference between predictive results and ground truth, NNG methods enable a more comprehensive understanding of subsurface conditions.

Compared to GNN-based NNG and CNN-based NNG, MLP-based NNG is mesh-independent, which results in reduced computational demands and higher efficiency (Hillier et al., 2023). In the GNN-based NNG approach, a tetrahedron mesh must be generated to represent the graph structure, and the graph (including vertices and edges) must be preserved throughout the training process (Hillier et al., 2021). This approach ties the resolution to available computing resources, potentially limiting the model's resolution. Additionally, GNN-based NNG only predicts scalar values at the vertices of the tetrahedron mesh. For query points beyond these vertices, an additional interpolation is often employed, leading to an extracted iso-surface that is less smooth than that produced by other NNG approaches. In the CNN-based NNG approach, the resolution should be defined before training, the fixed resolution is one potential limitation of the model's flexibility. Besides, the CNN-based NNG approach generally requires a more complex architecture and higher computation costs. Due to these considerations, we focus on MLP-based NNG methods in the following.

Generally, the MLP-NNG approach has demonstrated promising performance. However, it cannot currently model faults effectively. There remains ambiguity in accurately representing the scalar value jump at fault locations, and in preventing spurious discontinuities.

In typical implicit geomodelling approaches, different strategies can be used for modelling faults. The first approach involves a Boolean operation at the fault interface, where the hanging wall and footwall are modelled using two separate implicit functions (Caumon et al., 2013). A limitation of this method is that the point information on either side of the fault interface cannot interact. The second approach integrates a discontinuous step function into the implicit function at the fault location (Calcagno et al., 2008; de la Varga et al., 2019). This method does not require pre-specified fault displacement, as it is computed by solving the co-kriging matrix. The third approach involves using a kinematic operator to restore the fault interface, with fault displacement determined by an ellipsoid range of interface observations (Grose et al., 2021a). Additionally, some researchers have achieved impressive results using process simulation methods, such as the finite element method (Irakarama et al., 2022) and the finite difference method (Irakarama et al., 2021). However, the mesh-based nature of these methods may limit their application to large

datasets and high-resolution requirements. However, incorporating the aforementioned methods into neural networks is challenging, as the backpropagation process in neural networks requires global differentiability in the computational process.

In this contribution, we present a fault feature encoding approach for modelling faults using the MLP-NNG approach. The fault information is parameterized as additional features of observation and query points, with fault features associated with coordinates serving as the final input features to the neural network. To the best of our knowledge, this is the first work that employs a fault feature encoding method to represent faults in geomodelling. One advantage of this approach is that only fault location needs to be given before training the neural network, while the displacement of faults will be automatically learned during the training phase of the model. The key to fault feature encoding lies in identifying the relative position of the observation points and query points concerning the fault interface, and we introduce and compare three methods for this purpose. Additionally, we discuss a comparison in modelling fault with NNG among Boolean operations, discontinuous activation functions, and fault feature encoding approaches.

The remainder of this paper is organized as follows: Sect. 2 outlines the proposed methodology for modelling faults using fault feature encoding. Sect. 3 presents the modelling results using both a synthetic dataset and a real-world dataset. Sect. 4 discusses the characteristics of the proposed approach and compares it with other methodologies. Finally, Sect. 5 provides the conclusion.

2. Methodology

In this section, we introduce a novel fault modelling approach that utilizes fault feature encoding in the MLP-NNG framework. This approach leverages the inherent data-driven nature of neural networks and their ability to learn high-dimensional features. In our approach, each fault is associated with an additional feature assigned to all observations and query points. The number of additional features corresponds to the number of faults. The coordinates and fault features are then concatenated and used as inputs to a neural network, which outputs a predictive scalar field. The geological structure can be obtained by extracting the iso-surface from this scalar field. It is important to note that this method uses the same assumption as previous works' assumption where the approach requires prior knowledge of fault locations which are used to define the boundaries of the fault features.

2.1. Neural network geomodelling architecture

In the introduction, we described the various approaches to using neural networks in combination with implicit neural representations. We base the following work on the approach using MLP in the GeoINR proposed by (Hillier et al., 2023). As shown in Fig. 1, the input data consists of two components: the coordinates of interface indicator

points and orientations (as in the GeoINR), and additional fault encoding features (included in our work). These components are concatenated to form the neural network input. In neural networks, it is essential to calculate the difference between predicted outcomes and actual values, which is minimized through gradient descent to determine the optimal neural network parameters—effectively capturing the implicit mapping of the target scalar field. To achieve this, observation points across different interfaces are assigned distinct scalar values within the range of $[-1,1]$, with younger interfaces being assigned higher scalar values than older ones. To better preserve the characteristics of observations and fault geometry, the input features are duplicated and concatenated with the hidden layer features. The output, represented by a one-dimensional feature, corresponds to the predicted scalar value. Since the implicit neural representation is resolution-independent, the predictive scalar field can be visualized at any grid resolution, with geological structures being represented through the extraction of iso-surfaces.

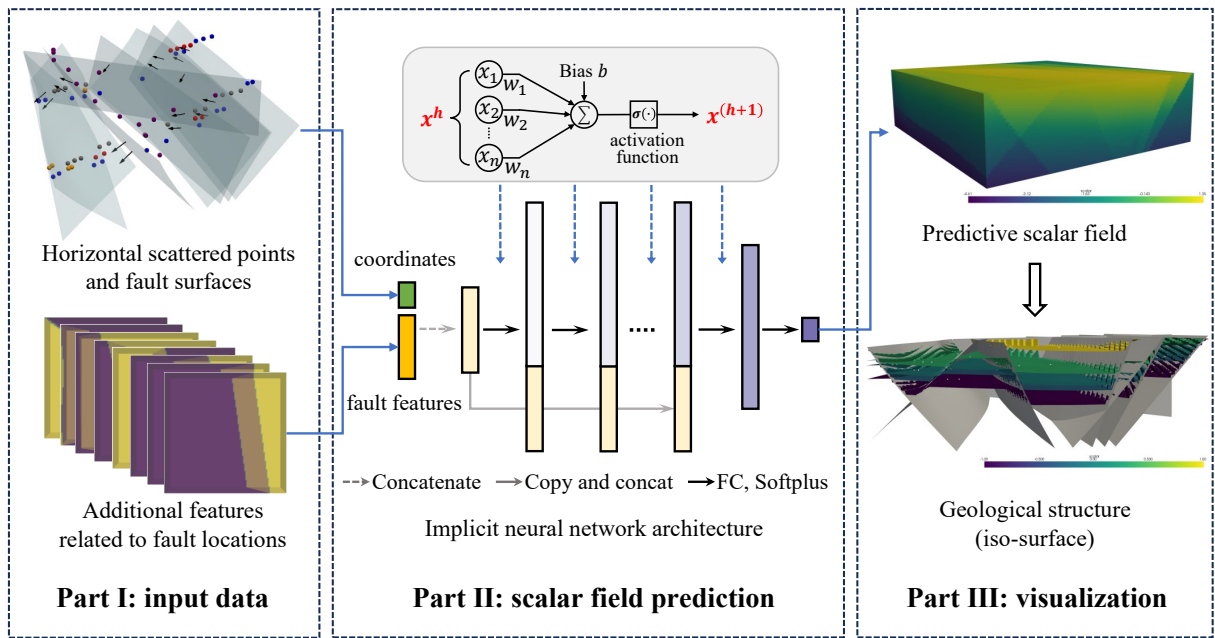


Figure 1: Illustration of fault modelling in implicit neural network. In part 1, faults are encoded as additional features, coordinates and fault features are concatenated to form the neural network input. Part 2 is the model training step, which is the same as GeoINR's training process. Part 3 is the visualization step, the geological structure represented by iso-surfaces.

For points with the same additional fault features, the only variation lies in their coordinates. As a result, the predictive scalar value field remains continuous and smooth beyond fault locations, with differences in values arising from spatial location variations. This behaviour is consistent with the principles observed in previous studies, regardless of whether using NNG or traditional interpolation methods. Around fault locations, the distinct fault features of points on either side of the fault help to identify scalar value discontinuities through a set of learnable parameters, which are described in the following.

2.2. Fault feature encoding

Feature values are critical for neural networks as neural networks learn the implicit function from the input features. The fault features of a point depend on the relative spatial relationship between the point and the faults. In this work, the fault surfaces are modelled firstly using the approach as in GeoINR. As demonstrated in previous studies (Hillier et al., 2021, 2023), the input features are normalized into the range of $[-1, 1]$ to facilitate the network's learning of useful latent representations and to produce accurate predictions. This normalization is essential in neural network training, particularly when the values of different input dimensions vary significantly. To align feature magnitude, it is necessary for fault feature values to also fall within this range. Maximizing the difference in feature values can further aid in the accurate identification of faults. Experimental results indicate that encoding the different sides of a fault using 0 and 1 is effective. For example, footwall for upward moving in normal fault setting is encoded as 1, while hanging wall for downward moving is encoded as 0 to reflect the fault movement trend.

To determine the locations of observation points and query points relative to the fault surface, we implement three different approaches:

- The first method utilizes the `select_enclosed_points` function from the PyVista package (Sullivan and Kaszynski, 2019). This approach involves creating an enclosed surface using the fault surface and model boundary, followed by traversing the points to assign feature values. Although this method is efficient, it occasionally misidentifies point locations. For instance, as illustrated in Fig. 2a, the point within the red circle is incorrectly identified, which can impact subsequent feature encoding and model training.
- The second method employs the `cKDTree` function from the SciPy package, which provides a rapid means of identifying the nearest neighbour point on the fault surface and then assigns feature values based on the spatial relationship between the points to be encoded and the nearest neighbour point of the fault surface. While this method is highly efficient, it can mistakenly identify points located on the boundary (Fig. 2b), resulting in an inaccurate representation of the fault in the subsequent predictive scalar field.
- The third method involves using the `compute_implicit_distance` function from the PyVista package. This function calculates the distance from observation or query points to the fault surface, where the point interior to the fault surface has a negative distance, the point exterior to the fault surface has a positive distance, and the point on the fault surface has a distance value of zero. This distance is then used to determine fault feature assignment. Although this method has a potential limitation in terms of efficiency, it accurately identifies points (Fig. 2c).

Due to the overall advantages and the stability of the approach, we adopt the third method for the subsequent case study. To simulate the ground truth more accurately, expert knowledge is employed to assess the relationships in

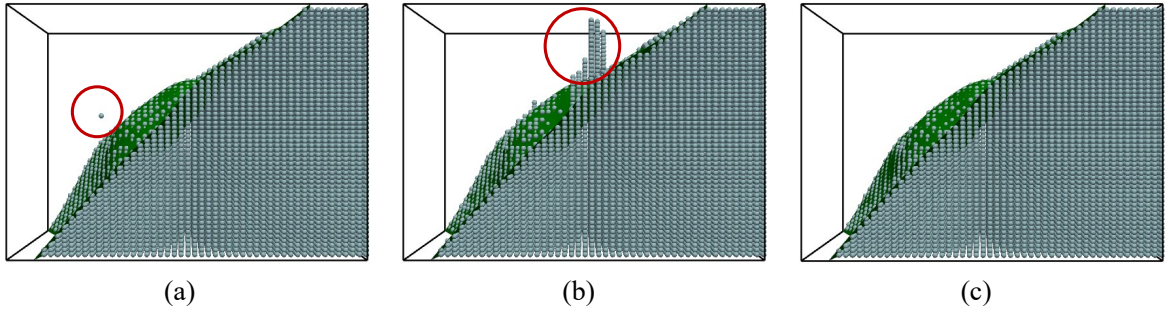


Figure 2: Illustration of three different methods for determining the spatial relationship of points relative to the fault surface. The green surface is the fault surface. The grey points are query points, here included to highlight the effect of the three methods, that should be located on the right side of the fault surface, in different sides of the fault will be assigned different feature values. The points inside the red circles indicate points will be incorrectly encoded fault features. (a) Identification result of using the `select_enclosed_points` function from the PyVista package. (b) Identification result of using the `cKDTree` function from the SciPy package. (c) Identification result of using the `compute_implicit_distance` from the PyVista package.

cross-cutting faults (Calcagno et al., 2008). For example, in Fig. 3a, the younger fault extends throughout the entire domain, making it straightforward to assign fault features, the younger fault features are shown in Fig. 3b. In contrast, the older fault is intersected by the younger fault and is present only in the block on the right side relative to the younger fault. Consequently, the fault features are assigned as shown in Fig. 3c, and the final features of this fault system as shown in Fig. 3d.

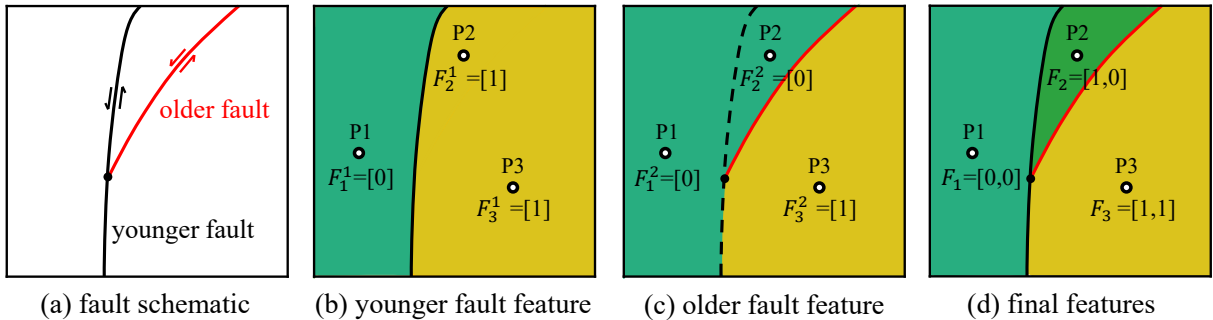


Figure 3: Fault feature encoding in cross-cutting faults. P1, P2, and P3 are three points in different spatial locations, F is the encoded fault features (e.g. $F_2^1 = [1]$ means the first fault feature in point P2 is 1, $F_2 = [1,0]$ means the final fault feature list in point P2 is $[1,0]$). (a) The fault schematic with a younger fault cutting an older fault, the arrows indicate the movement relationship between the hanging wall and foot wall. (b) Younger fault feature encoding, the point in the relatively moving down part with a 'green' colour is encoded feature '0', otherwise the encoded feature is '1'. (c) Couple expert knowledge to encode older fault features, the point in the 'green' part is encoded feature '0', otherwise the encoded feature is '1'. (d) The final fault features, the amount of fault features in each point depends on the amount of faults.

2.3. Constraints and loss functions

Neural networks offer a flexible framework for incorporating various geological constraints by minimizing the differences between predicted and actual values. Typical constraints in geomodelling include discrete interface indicator points and orientations. In the context of geological modelling using regression, mean squared error (MSE)

is commonly employed as a loss function to optimize neural network parameters, thereby ensuring that the predicted values converge to the ground truth. It is worth noting that MSE loss is sensitive to outliers, which makes an unsatisfactory modelling performance in the noise dataset (Bi et al., 2022). We find that accumulating the squared error as interface observation loss can achieve better modelling results than using MSE loss. This improvement may be due to a higher interface observation loss, which encourages the neural network to focus more on aligning the predicted interface with the interface observation's locations. Consequently, the loss function of interface points L_P can be expressed as:

$$L_P = \sum (\mathbf{y}_{\text{pred}} - \mathbf{y}_{\text{obs}})^2 \quad (1)$$

where \mathbf{y}_{pred} is the predictive scalar values of observation points, and \mathbf{y}_{obs} is the ground truth.

We reconstruct the geological modelling within a Cartesian coordinate system, where dip and azimuth were converted into a vector represented by (n_x, n_y, n_z) . The normal vector in the scalar field can be represented by the gradient of scalar value, for an iso-surface, the normal vector aligns with the scalar value gradient. Consequently, the loss function for orientation observations L_O is defined as:

$$L_O = \frac{1}{N} \sum_i^N \left(\cos\theta_i^{\text{pred}} - \cos\theta_i^{\text{obs}} \right)^2 \quad (2)$$

where N is the number of orientation points, $\cos\theta_i^{\text{pred}}$ is the cosine similarity between orientation observation and the gradient of the scalar field in a point. For normal orientation observation, the cosine similarity $\cos\theta_i^{\text{obs}} = 1$. The cosine similarity between predictive and ground true is defined as:

$$\cos\theta_i^{\text{pred}} = \frac{\mathbf{n}_i \cdot \nabla z_i^{\text{scalar}}}{\|\mathbf{n}_i\| \|\nabla z_i^{\text{scalar}}\|} \quad (3)$$

where \mathbf{n}_i is orientation observation vector, $\nabla z_i^{\text{scalar}}$ is the gradient of the scalar field in a point.

To calculate the gradient at a point, automatic differentiation in TensorFlow or PyTorch can directly be employed to compute the partial derivatives of the predictive scalar field with respect to the coordinate components in the x, y, z directions. The normalized partial derivatives in this context correspond to $\nabla z_i^{\text{scalar}}$.

In some datasets, interface observation points are close to the fault surface and if only fault observations themselves are used to model the fault, the modelled fault interface may be unreasonable, as shown in Fig. 4. In such a case, it is possible to constrain the 'above' and 'below' relationship to prevent the modelled interface from incorrectly

segmenting different blocks. The loss functions of spatial relationships are defined as:

$$L_{above} = \sum_i^N \delta_{z_i, I^{scalar}}, \delta_{z_i, I^{scalar}} = \begin{cases} |z_i - I^{scalar}|, z_i - I^{scalar} < 0 \\ 0, z_i - I^{scalar} \geq 0 \end{cases} \quad (4)$$

$$L_{below} = \sum_i^N \delta_{z_i, I^{scalar}}, \delta_{z_i, I^{scalar}} = \begin{cases} z_i - I^{scalar}, z_i - I^{scalar} > 0 \\ 0, z_i - I^{scalar} \leq 0 \end{cases} \quad (5)$$

where z_i is the scalar value corresponding to a point, I^{scalar} is the iso-value of an interface. $\delta_{z_i, I^{scalar}}$ is the scalar value difference between a point and an interface. The final loss function is an accumulation of all kinds of loss functions with different coefficients.

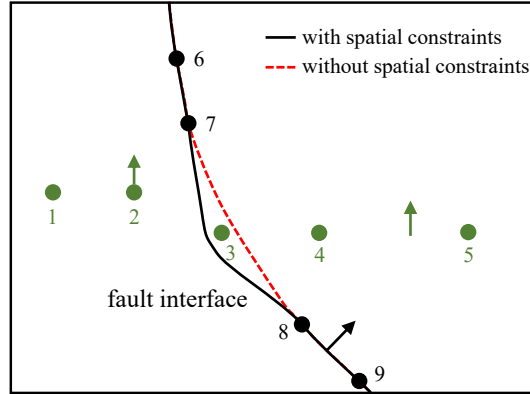


Figure 4: The effect of using spatial constraints (L_{above} and L_{below}) when modelling the fault surface. The points and arrows represent the interface observations and orientation observations respectively. The observations with a 'black' colour are from the fault and observations with a 'green' colour from a stratigraphic interface. In the presented approach, the scalar value at points 3, 4, and 5 should be larger than the iso-value of the fault interface, which means points 3, 4, and 5 are located above the fault interface in the scalar field. Without using the spatial constraints, the modelled fault surface is represented by the dot red line, where point 3 is wrong located. The solid black line represents the reasonable fault interface.

3. Case studies

To test the fault feature encoding method for modelling faults in an NNG framework, as previously described, both a synthetic and a real-world case were employed. For both case studies, the learnable parameters of the neural network were initialized randomly within the PyTorch framework. Due to the variation in results caused by different neural network parameter initializations, a random seed was set to ensure the reproducibility of the numerical outcomes. The hyperparameters of the NNG used in both cases are summarized in Table 1. The optimizer utilized is Adam, and the

Table 1

Model parameter values for case studies.

Parameters	Synthetic Model	Gullfaks Field Model
Number of hidden layers	2	2
Dimension of hidden layers	256	512
Learning rate	0.001	0.001
Activation function	Softplus ($\beta = 1$)	Softplus ($\beta = 210$)
Training epochs	1000	1000
Inference voxel grid size	100x100x100	100x100x100

nonlinear activation function employed is the Softplus function:

$$\sigma(x) = \frac{1}{\beta} \log(1 + e^{\beta x}) \quad (6)$$

where β is a hyperparameter that controls the shape of the objective interface. Smaller values of β result in flatter modelled interfaces, while higher values yield more locally variant interfaces. This parameter is not only useful for smoothing of the interface itself, but also to reduce the effect of interface point variances in dense datasets. The default value of β is set to 1. It is noteworthy that the Softplus function, when used with a large β value, serves as a smooth approximation to the commonly used ReLU activation function. In contrast to the ReLU function, which is undifferentiable at zero, the Softplus function is globally differentiable, thereby yielding smoother modelled interfaces.

After training using the geological observations, a uniform grid mesh was used for inference. Scalar field values were assigned to each vertex in the grid, allowing for the representation of the geological structure by extracting the iso-surface. The results presented were obtained using a single NVIDIA RTX 3070 GPU.

3.1. Synthetic model

The first case study involves a synthetic layer cake model consisting of five stratigraphic layers intersected by two faults. The older fault is a semi-infinite fault that is cut off by the younger fault, and it exists only within the hanging wall of the younger fault. As illustrated in Fig. 5a, the observations include 54 interface points from four distinct interfaces and 10 orientations in total. Based on the observational data, the strata are likely to be (sub-)horizontal; therefore, the beta parameter in the Softplus activation function was set to a low value. In this case, a beta value of 1 was chosen to ensure that the modelled interfaces remained horizontal. Three sub-domains were generated through fault segmentation, with additional fault features assigned as [0,1], [0,0], and [1,0] in each sub-domain respectively. The first value in the fault features corresponds to the younger fault, the second value corresponds to the older fault. The hyperparameters for the NNG used in the synthetic model are listed in Table 1. The training epoch was set to 1000, indicating that the learnable parameters of the neural network were updated 1000 times through feed-forward prediction and backpropagation.

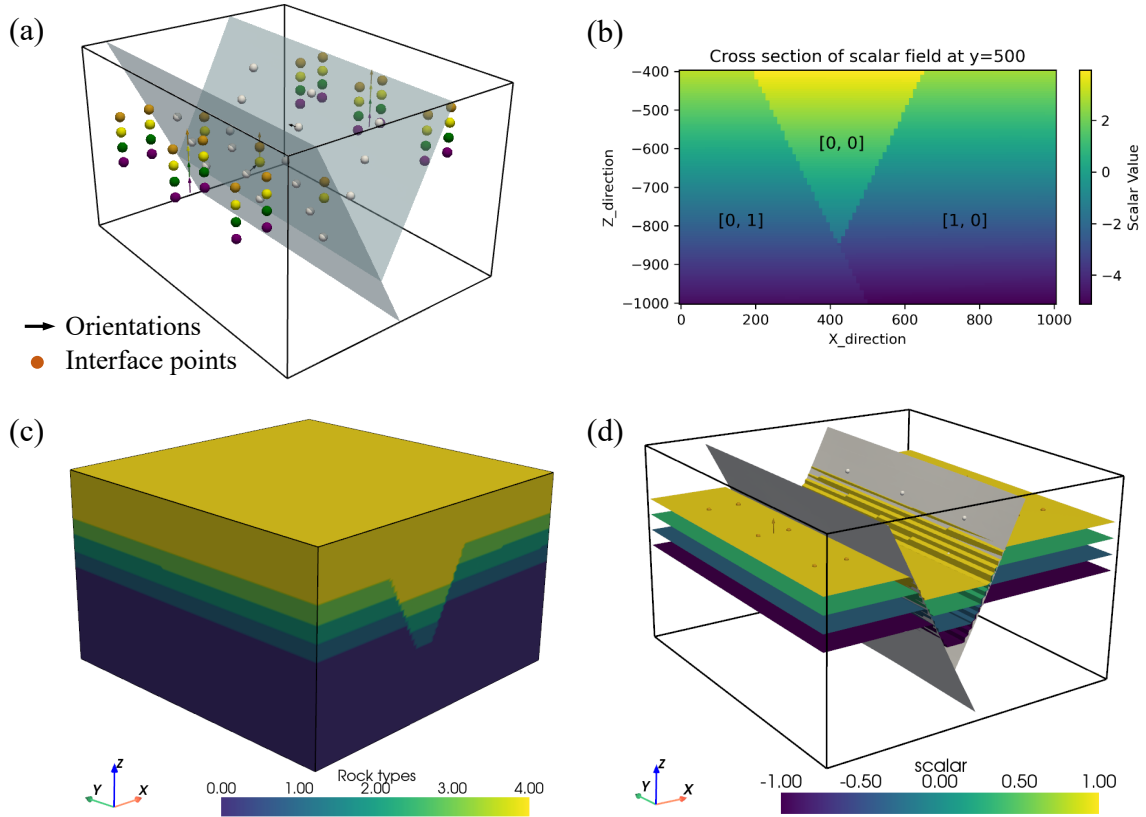


Figure 5: Modelling result of the synthetic model. (a) Visualization of observation data. (b) Cross-section of a scalar field, and associated fault feature in each subdomain. (c) Predictive rock units. (d) Extracting iso-surface as a modelled geological structure.

Table 2

Model performance metrics for case studies.

Model	Metric	Value
Synthetic model (with semi-infinite fault) - 54 interface points - 10 orientation points	Interface loss	5.001e-4
	Orientation loss	6.002e-5
	Per-epoch training time	1.79ms
	Inference time for voxel grid	0.06s
Gullfaks field model (fault and unconformity) - 395 interface points - 145 orientation points	Interface loss	4.822e-1
	Orientation loss	5.115e-1
	Per-epoch training time	2.24ms
	Inference time for voxel grid	3.06s

Model performance was evaluated based on predictive loss, training time, and inference time, as detailed in Table 2. The predictive value is the scalar field value associated with each vertex on the voxel grid, allowing the final predictive scalar field to be easily visualized using PyVista. Fig. 5b shows a cross-section of the predictive scalar field corresponding to the assigned fault features. By defining specific iso-values, the stratigraphy can be characterized by different rock types (Fig. 5c), and iso-surfaces can be extracted to represent the predictive geological structure (Fig. 5d).

3.2. Gullfaks field model

The second case study uses a real-world dataset from a part of the Gullfaks field, located in the northern North Sea. The field is in the western part of the Viking Graben and consists of the NNE-SSW-trending 10 – 25 km wide Gullfaks fault block. The original and detailed regional and structural geology refers to Fossen and Hesthammer (1998), this case using an interpreted and simplified sub-dataset from Schaaf et al. (2021).

The simplified model of the Gullfaks field includes two faults, three horizon tops (Tarbert – yellow, Ness – green, and Etive – purple), and the Base Cretaceous Unconformity (BCU, red), as illustrated in Fig. 6a. As discussed in Section 2, feature encoding for fault modelling in NNG requires knowledge of the fault’s location and geometry. Therefore, the two fault surfaces in the Gullfaks field model must first be established. Given that the feature dimensions for fault modelling and unconformity modelling differ, the fault modelling process incorporates two additional fault features beyond the standard coordinate features, but unconformity modelling only needs to use the coordinates as neural network input features. Consequently, the unconformity process needs to be modelled separately.

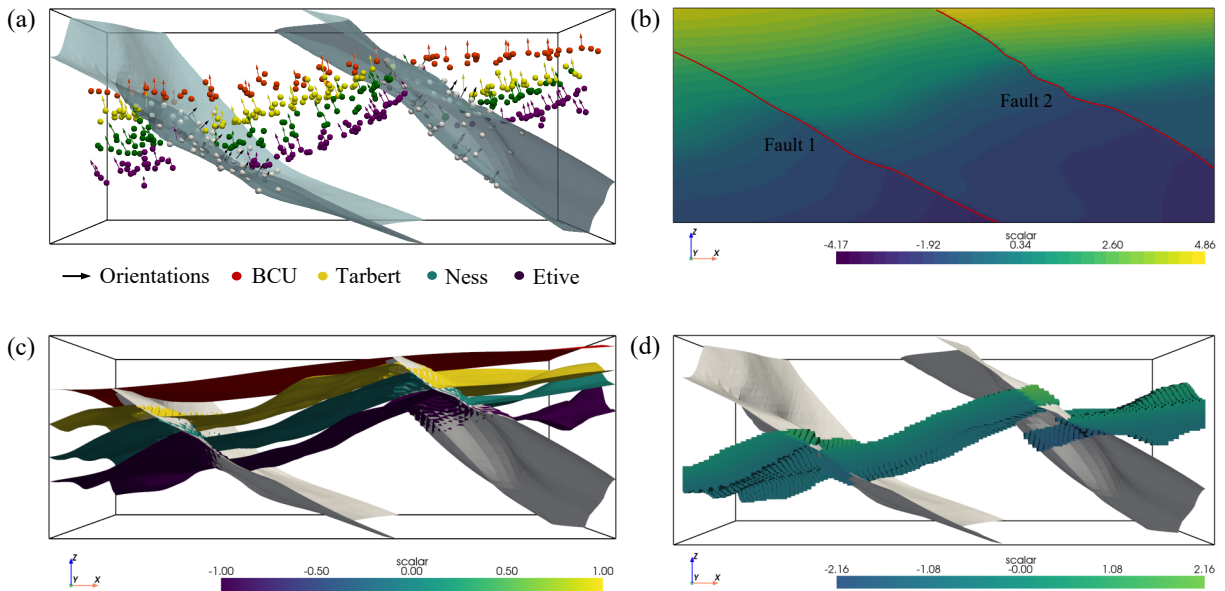


Figure 6: Modelling result of Gullfaks field model. (a) Visualization of observation data. (b) Predictive scalar field without unconformity, faults are treated as infinite faults. (c) Extracting iso-surface as modelled geological structure, unconformity interface was modelled individually. (d) Visualization of the ‘Ness’ layer.

Based on the observations, the target interfaces exhibit local variability, and a high beta value for the Softplus activation function is recommended to capture these local features effectively. A beta value of 210 has been found experimentally to strike an effective balance between global smoothness and local variability. In the absence of unconformities, faults are treated as infinite, simplifying the encoding of fault features. These fault features are assigned values of [1,1], [0,1], and [0,0] respectively, based on their locations. The hyperparameters of the NNG used in the Gullfaks field model are provided in Table 1. Model performance metrics, including constraint predictive loss,

training time, and inference time, are detailed in Table 2.

The final modelled geological structure is shown in Fig. 6c. To achieve this, the iso-surface mesh was first extracted from the predictive scalar field (Fig. 6b), and then the `clip_surface` function in Pyvita was employed to remove extraneous fault and iso-surface meshes according to the unconformity interface. Additionally, due to the implicit interpolation approach, it is straightforward to estimate voxels of stratigraphic layers for visualisation and further computation (Fig. 6d).

4. Discussion

4.1. Advantages of fault feature encoding approach

In the implicit scalar field, a discontinuous jump in scalar value should occur at fault positions, representing the displacement caused by stratigraphic movement. However, gradient-based optimization struggles to enable standard neural networks to precisely locate discontinuities. Coordinate-based neural networks, in particular, often fail to accurately capture these discontinuities in the implicit field, leading to smoothed representations (Belhe et al., 2023), as illustrated in Fig. 7a. Accurately representing discontinuities in neural networks remains a significant challenge. In 3D implicit geomodelling, three primary approaches are commonly used to integrate faults into implicit models: Boolean operations (Laurent et al., 2013), step functions (Calcagno et al., 2008; de la Varga et al., 2019), and kinematic methods (Grose et al., 2021a).

In the context of Boolean operations in MLP-NNG, the subdomains on different sides of a discontinuity are represented by two distinct implicit functions. The Boolean operation, defined by the discontinuity location, determines which function is employed to represent the discontinuity. This implies that observations on either side of the discontinuity are treated independently and are modelled separately, leading to inconsistent trends on both sides across the discontinuity, as illustrated in Figure 7b. This approach is incompatible with geological settings, where the properties (e.g., geometry) of stratigraphy are assumed to be consistent across both sides of a fault. Proper modelling of geological structures requires considering the interaction between observations on both sides of the fault, a consideration that the Boolean operation method fails to address. Additionally, Boolean operations are computationally intensive, as each subdomain divided by faults must be modelled individually. This approach becomes particularly time-consuming when dealing with complex fault systems.

A step function is an effective method for describing a discontinuity function, which characterizes a value jump at a discontinuity location. A typical application of this approach in geomodelling can be found in GemPy (de la Varga et al., 2019). To integrate a step function into a neural network, a Heaviside function was incorporated into the neural network's activation function to capture the discontinuity (Della Santa and Pieraccini, 2023), the activation function

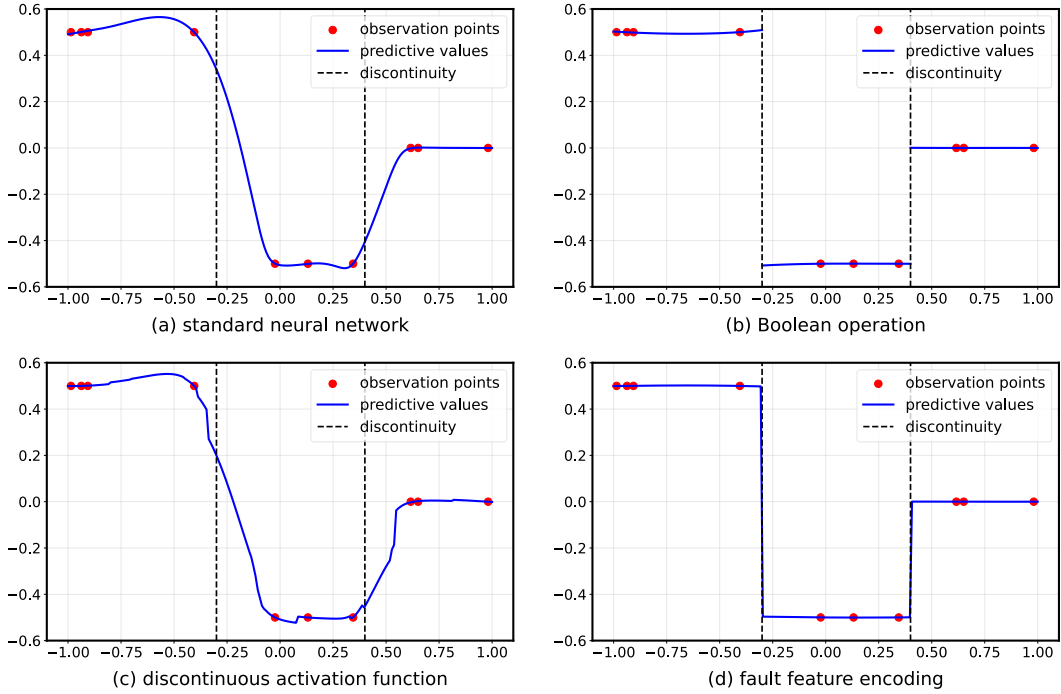


Figure 7: Schematic diagram of different discontinuity modelling methods in the neural network. Using 10 randomly sampled points to fit a piecewise function, the discontinuities are located at -0.3 and 0.4. All methods use the same parameter (learning rate is 0.01, activation function is Softplus (beta=10)).

can be expressed as:

$$\mathbf{x}^{(h+1)} = f_{h+1}(\mathbf{W}^{(h+1)}\mathbf{x}^{(h)} + \mathbf{b}^{(h+1)}) + \varepsilon^{(h+1)} \cdot H(\mathbf{W}^{(h+1)}\mathbf{x}^{(h)} + \mathbf{b}^{(h+1)}) \quad (7)$$

where f is a general activation function, it can be any commonly used activation function. ε is a new parameter of the neural network, it learns the displacement of discontinuity. H refers to the Heaviside step function.

Formula 7 simplifies the Heaviside function as a constant function during backpropagation, which is not strictly accurate because the Heaviside function is non-differentiable in discontinuous value. A potential method to address this limitation is to use smooth approximations, such as the sigmoid function, to make the discontinuous activation function differentiable. One limitation of employing a discontinuous activation function is that it requires dense observations for fitting and necessitates observations close to the discontinuity location. However, in geomodelling scenarios, observation points are typically discrete and sparse.

It is worth noting that not all new datasets or domain knowledge need to be encoded as additional features. An alternative approach is to use physics-informed neural networks (PINNs) to guide the variation of the scalar field. This method approximates solutions to partial differential equation problems by designing a loss function derived directly from the differential equation (Karniadakis et al., 2021; Raissi et al., 2017). In this study, the Heaviside

function (or a sigmoid function variant to preserve sharp transitions at discontinuous locations while maintaining global differentiability) is a possible approach to describe stratigraphic displacement by designing a discontinuous activation function. However, directly using such a discontinuous activation function without specifying the fault location may lead to erroneous predictions, as unexpected faults in conformable stratigraphy could result in incorrect predictions. Additionally, discontinuities may not align with domain boundaries, as illustrated in Fig. 7c. This makes it challenging to accurately locate the position of sharp transitions and may result in spurious discontinuities. Revisiting Eq. (7), it is evident that the activation function merely transforms the predictive value without establishing a connection to the discontinuity location. Consequently, for the neural network, there could be multiple potential discontinuity locations that might allow the predictive curve to fit the observation points.

Moreover, when the fault location is known, the primary challenge lies in constraining the displacement distance. In Fig. 8, the true jump value in location 0 is 10 in the synthetic dataset; however, when the indicated displacement value for the discontinuous activation function is either too large or too small, it fails to accurately capture the sharp transitions at the discontinuity location. An approximation method that involves aligning the fault using a volumetric vector field and calculating the fault displacement can be employed, by such a method referred to by Godefroy et al. (2018), Grose et al. (2021a), and Laurent et al. (2013). However, this displacement approximation may be unprecise where the observation interface points are sparse around the fault.

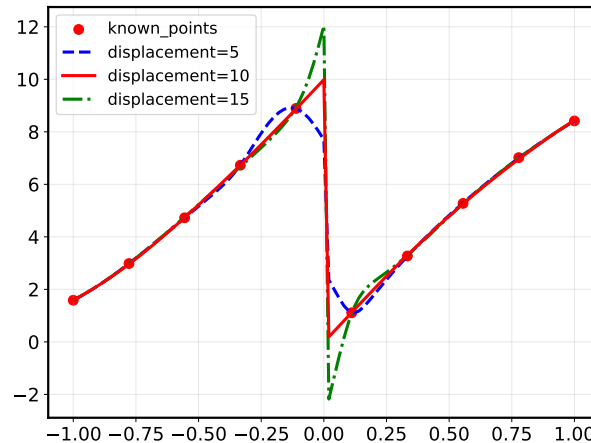


Figure 8: Effect of indicated displacement for discontinuity activation function, all the fitting results using the same neural network hyper-parameters and learnable parameter initialization, the difference only comes from indicated displacement.

With the fault feature encoding approach used in this work, it is only required to know the location of the fault, as the displacement itself is learned by the neural network. The modelling results in Fig. 7d demonstrate the approach's ability to model discontinuities, with the sharp transitions preserved, the discontinuities accurately located, and the curve maintaining continuity at the boundaries. In our experiments, modelling fault with the neural network, the fault feature encoding method generally outperforms the Boolean operation and the using a discontinuous activation

function.

4.2. Modelling finite faults

In the case of the synthetic model, there exists a semi-infinite fault that is truncated by a younger fault. Assigning fault features to observation and query points is straightforward when using the same rule as for an infinite fault. Nonetheless, if the finite fault is entirely contained within the model without intersecting any other faults or the model bounding box, encoding the fault features becomes more complex. Belhe et al. presented a novel framework to capture and represent discontinuity using a neural network in a 2D scenario (Belhe et al., 2023). This approach first applies robust curved triangulation for assigning one or more features to a triangle mesh vertex. For vertices next to discontinuity curves, assigning a feature for each side of every discontinuity; for vertices in the continuous domain, only one feature is assigned. The query points assigned features by interpolating the vertex features. It should be interesting to introduce this discontinuity-aware approach to model any form of finite fault by fault feature encoding in the MLP-NNG framework.

4.3. Potential opportunity for integrating geophysics data and domain knowledge

Incorporating updated data and domain knowledge into the input of an NNG is a convenient way to impose constraints to make a comprehensive prediction (Wu et al., 2023). Previous results have demonstrated the capability of the fault feature encoding approach to support fault modelling using the MLP-NNG framework. This approach integrates fault features from observation points or query points as domain knowledge. As a data-driven computational method, NNG benefits significantly from rich feature sets; increased detail in point features generally leads to more precise modelling outcomes. Furthermore, the NNG method is highly efficient during the inference step, which functions similarly to surrogate modelling. The training process focuses on observational points, while query points can be mapped using the trained network. The success of integrating fault features into the modelling process encourages us to continuously update the model by integrating gradually updated data and domain knowledge, encoding rock property and geomechanics data as features that could potentially explain spatial variations in the subsurface.

Another advantage of using NNG is that this kind of approach employs gradient-based optimization, providing a natural framework for integrating geophysical forward simulations. Recent studies have demonstrated the use of differential geomodelling approaches to integrate geological modelling methods with gradient-based geophysical inversion techniques (Shen et al., 2023; Wellmann et al., 2024). Differentiable models are particularly valuable for accurately and efficiently computing gradients with respect to model input features or parameters, enabling the discovery of high-dimensional unknown relationships. Geophysics data offer significant benefits, including rich datasets and low acquisition costs, as exemplified by gravity and magnetic data, which provide additional evidence of subsurface conditions. These attributes make geophysics data particularly suitable for data-driven geomodelling approaches.

There have been several studies on geophysical forward modelling and inversion using deep neural networks (Huang et al., 2021; Yu and Ma, 2021).

Our work extends the capability of the MLP-NNG framework to represent fault structures, thereby offering an opportunity to integrate geological modelling with gradient-based geophysical inversion in more complex geological settings. Since both geophysical inversion and NNG approaches utilize gradients to approach observational data, for integrating gravity data into geological modelling, one could use the predictive geological structure by the NNG approach to conduct a gravity forward simulation, using the residual between predictive gravity and measured gravity as an additional loss function using for backpropagation, which can be an end-to-end framework.

4.4. Limitations

It should be noted that the initialization of neural network parameters significantly influences the predictive scalar field. When using random initialization for model parameters, different runs will come out similar but not with the same result. To enhance the reproducibility of predictions, setting a random seed or using pre-trained model parameters (Hillier et al., 2023) are commonly used. However, even under these conditions, the predictive result represents only one of the possible realizations. In other words, when using a neural network for modelling, the inherent uncertainty of the network parameters propagates to the predictive results. To estimate this uncertainty, approaches such as Bayesian neural networks (Blundell et al., 2015; Gal and Ghahramani, 2015) or an ensemble method (Lakshminarayanan et al., 2016) can be employed. Moreover, feature encoding is highly dependent on the fault interface position. However, in a realistic setting, also the uncertainty of the fault position could be considered, for example combining the interpolation method shown here with a probabilistic modeling approach (Wellmann and Caumon, 2018). The primary purpose of this work is to demonstrate the feasibility of the fault encoding method within the context of the NNG framework; hence, a determined fault interface was utilized to simplify the process.

As the interface loss and orientation loss typically differ in magnitude, it is important to balance the contributions of L_P and L_O to identify the optimal combined loss function. In the case studies, we simply set the coefficients of L_P , L_O , L_{above} , and L_{below} as 1. However, manually setting the coefficients can't find the optimal balance of different losses. To address this issue, it may be worthwhile to explore the possibility of setting the coefficient as a learnable parameter within a neural network, allowing for adaptive optimization (Li and Feng, 2022).

5. Conclusions

Faults are important geological structures with high relevance to a wide range of practical applications and, therefore, often need to be considered in 3D geological models. This contribution extends the modelling capabilities of the existing MLP-NNG framework, using a fault feature encoding strategy to model fault within this context. The

results demonstrate the presented approach's ability to generate a reasonable scalar field and preserve sharp transition in fault location. Compared to the use of discontinuous activation functions and Boolean operations, the proposed approach is more efficient and easier to implement. Furthermore, the feature encoding method in the MLP-NNG framework offers a promising opportunity to integrate prior domain knowledge and geophysics datasets into structural modelling.

Acknowledgments

The China Scholarship Council (CSC) is acknowledged for supporting the first author of this paper financially. We gratefully acknowledge and appreciate the insightful discussions with Michael Hillier from the Geological Survey of Canada, and we extend our thanks to MH for his valuable comments on this manuscript. We thank David Nathan from RWTH Aachen University for his advice on this manuscript. Additionally, we are thankful for all the discussions with colleagues from RWTH Aachen University.

References

- Belhe, Y., Gharbi, M., Fisher, M., Georgiev, I., Ramamoorthi, R., Li, T.M., 2023. Discontinuity-Aware 2D Neural Fields. *ACM Transactions on Graphics* 42, 1–11. doi:10.1145/3618379.
- Bi, Z., Wu, X., Li, Z., Chang, D., Yong, X., 2022. DeepISMNet: three-dimensional implicit structural modeling with convolutional neural network. *Geoscientific Model Development* 15, 6841–6861. doi:10.5194/gmd-15-6841-2022.
- Blundell, C., Cornebise, J., Kavukcuoglu, K., Wierstra, D., 2015. Weight Uncertainty in Neural Networks doi:10.48550/ARXIV.1505.05424.
- Calcagno, P., Chilès, J., Courrioux, G., Guillen, A., 2008. Geological modelling from field data and geological knowledge. *Physics of the Earth and Planetary Interiors* 171, 147–157. doi:10.1016/j.pepi.2008.06.013.
- Carr, J.C., Beatson, R.K., Cherrie, J.B., Mitchell, T.J., Fright, W.R., McCallum, B.C., Evans, T.R., 2001. Reconstruction and representation of 3D objects with radial basis functions, in: *Proceedings of the 28th annual conference on Computer graphics and interactive techniques*, ACM. pp. 67–76. doi:10.1145/383259.383266.
- Caumon, G., Gray, G., Antoine, C., Titeux, M.O., 2013. Three-Dimensional Implicit Stratigraphic Model Building From Remote Sensing Data on Tetrahedral Meshes: Theory and Application to a Regional Model of La Popa Basin, NE Mexico. *IEEE Transactions on Geoscience and Remote Sensing* 51, 1613–1621. doi:10.1109/TGRS.2012.2207727.
- Della Santa, F., Pieraccini, S., 2023. Discontinuous neural networks and discontinuity learning. *Journal of Computational and Applied Mathematics* 419, 114678. doi:10.1016/j.cam.2022.114678.
- Fossen, H., Hesthammer, J., 1998. Structural geology of the Gullfaks Field, northern North Sea. Geological Society, London, Special Publications 127, 231–261. doi:10.1144/GSL.SP.1998.127.01.16.
- Gal, Y., Ghahramani, Z., 2015. Dropout as a Bayesian Approximation: Representing Model Uncertainty in Deep Learning. doi:10.48550/ARXIV.1506.02142.
- Godefroy, G., Caumon, G., Ford, M., Laurent, G., Jackson, C.A.L., 2018. A parametric fault displacement model to introduce kinematic control into modeling faults from sparse data. *Interpretation* 6, B1–B13. doi:10.1190/INT-2017-0059.1.
- Gonçalves, t.G., Guadagnin, F., Cordova, D.P., 2022. Learning spatial patterns with variational Gaussian processes: Regression. *Computers & Geosciences* 161, 105056. doi:10.1016/j.cageo.2022.105056.

- Gonçalves, t.G., Guadagnin, F., Cordova, D.P., 2023. Variational Gaussian processes for implicit geological modeling. *Computers & Geosciences* 174, 105323. doi:10.1016/j.cageo.2023.105323.
- Gonçalves, t.G., Kumaira, S., Guadagnin, F., 2017. A machine learning approach to the potential-field method for implicit modeling of geological structures. *Computers & Geosciences* 103, 173–182. doi:10.1016/j.cageo.2017.03.015.
- Grose, L., Ailleres, L., Laurent, G., Caumon, G., Jessell, M., Armit, R., 2021a. Modelling of faults in LoopStructural 1.0. *Geoscientific Model Development* 14, 6197–6213. doi:10.5194/gmd-14-6197-2021.
- Grose, L., Ailleres, L., Laurent, G., Jessell, M., 2021b. LoopStructural 1.0: time-aware geological modelling. *Geoscientific Model Development* 14, 3915–3937. doi:10.5194/gmd-14-3915-2021.
- Guo, J., Xu, X., Wang, L., Wang, X., Wu, L., Jessell, M., Ogarko, V., Liu, Z., Zheng, Y., 2024. GeoPDNN 1.0: a semi-supervised deep learning neural network using pseudo-labels for three-dimensional shallow strata modelling and uncertainty analysis in urban areas from borehole data. *Geoscientific Model Development* 17, 957–973. doi:10.5194/gmd-17-957-2024.
- Hillier, M., Wellmann, F., Brodaric, B., de Kemp, E., Schetselaar, E., 2021. Three-Dimensional Structural Geological Modeling Using Graph Neural Networks. *Mathematical Geosciences* 53, 1725–1749. doi:10.1007/s11004-021-09945-x.
- Hillier, M., Wellmann, F., De Kemp, E.A., Brodaric, B., Schetselaar, E., Bédard, K., 2023. GeoINR 1.0: an implicit neural network approach to three-dimensional geological modelling. *Geoscientific Model Development* 16, 6987–7012. doi:10.5194/gmd-16-6987-2023.
- Hillier, M.J., Schetselaar, E.M., de Kemp, E.A., Perron, G., 2014. Three-Dimensional Modelling of Geological Surfaces Using Generalized Interpolation with Radial Basis Functions. *Mathematical Geosciences* 46, 931–953. doi:10.1007/s11004-014-9540-3.
- Huang, R., Liu, S., Qi, R., Zhang, Y., 2021. Deep Learning 3D Sparse Inversion of Gravity Data. *Journal of Geophysical Research: Solid Earth* 126, e2021JB022476. doi:10.1029/2021JB022476.
- Irakarama, M., Laurent, G., Renaudeau, J., Caumon, G., 2021. Finite Difference Implicit Structural Modeling of Geological Structures. *Mathematical Geosciences* 53, 785–808. doi:10.1007/s11004-020-09887-w.
- Irakarama, M., Thierry-Coudon, M., Zakari, M., Caumon, G., 2022. Finite Element Implicit 3D Subsurface Structural Modeling. *Computer-Aided Design* 149, 103267. doi:10.1016/j.cad.2022.103267.
- Karniadakis, G.E., Kevrekidis, I.G., Lu, L., Perdikaris, P., Wang, S., Yang, L., 2021. Physics-informed machine learning. *Nature Reviews Physics* 3, 422–440. doi:10.1038/s42254-021-00314-5.
- Lajaunie, C., Courrioux, G., Manuel, L., 1997. Foliation fields and 3D cartography in geology: Principles of a method based on potential interpolation. *Mathematical Geology* 29, 571–584. doi:10.1007/BF02775087.
- Lakshminarayanan, B., Pritzel, A., Blundell, C., 2016. Simple and Scalable Predictive Uncertainty Estimation using Deep Ensembles. doi:10.48550/ARXIV.1612.01474.
- Laurent, G., Caumon, G., Bouziat, A., Jessell, M., 2013. A parametric method to model 3D displacements around faults with volumetric vector fields. *Tectonophysics* 590, 83–93. doi:10.1016/j.tecto.2013.01.015.
- Li, S., Feng, X., 2022. Dynamic Weight Strategy of Physics-Informed Neural Networks for the 2D Navier–Stokes Equations. *Entropy* 24, 1254. doi:10.3390/e24091254.
- Mallet, J.L., 1992. Discrete smooth interpolation in geometric modelling. *Computer-Aided Design* 24, 178–191. doi:10.1016/0010-4485(92)90054-E.
- Mallet, J.L., 1997. Discrete modeling for natural objects. *Mathematical Geology* 29, 199–219. doi:10.1007/BF02769628.
- Pyrzc, M., Deutsch, C.V., 2014. *Geostatistical reservoir modeling*. Second edition ed., New York, New York : Oxford University Press, Oxford.
- Raissi, M., Perdikaris, P., Karniadakis, G.E., 2017. *Physics Informed Deep Learning (Part I): Data-driven Solutions of Nonlinear Partial Differential*

Equations. doi:10.48550/ARXIV.1711.10561.

- Ringrose, P., Bentley, M., 2015. Reservoir Model Design: A Practitioner's Guide. Springer Netherlands, Dordrecht. doi:10.1007/978-94-007-5497-3.
- Schaaf, A., De La Varga, M., Wellmann, F., Bond, C.E., 2021. Constraining stochastic 3-D structural geological models with topology information using approximate Bayesian computation in GemPy 2.1. Geoscientific Model Development 14, 3899–3913. doi:10.5194/gmd-14-3899-2021.
- Shen, C., Appling, A.P., Gentine, P., Bandai, T., Gupta, H., Tartakovsky, A., Baity-Jesi, M., Fenicia, F., Kifer, D., Li, L., Liu, X., Ren, W., Zheng, Y., Harman, C.J., Clark, M., Farthing, M., Feng, D., Kumar, P., Aboelyazeed, D., Rahmani, F., Song, Y., Beck, H.E., Bindas, T., Dwivedi, D., Fang, K., Höge, M., Rackauckas, C., Mohanty, B., Roy, T., Xu, C., Lawson, K., 2023. Differentiable modelling to unify machine learning and physical models for geosciences. Nature Reviews Earth & Environment doi:10.1038/s43017-023-00450-9.
- Sullivan, C., Kaszynski, A., 2019. PyVista: 3D plotting and mesh analysis through a streamlined interface for the Visualization Toolkit (VTK). Journal of Open Source Software 4, 1450. doi:10.21105/joss.01450.
- de la Varga, M., Schaaf, A., Wellmann, F., 2019. GemPy 1.0: open-source stochastic geological modeling and inversion. Geoscientific Model Development 12, 1–32. doi:10.5194/gmd-12-1-2019.
- Wellmann, F., Caumon, G., 2018. 3-D Structural geological models: Concepts, methods, and uncertainties, in: Advances in Geophysics. Elsevier. volume 59, pp. 1–121. doi:10.1016/bs.agph.2018.09.001.
- Wellmann, F., De La Varga, M., Liang, Z., 2024. Differentiable Geomodeling: towards a tighter implementation of structural geological models into geophysical inverse frameworks. doi:10.5194/egusphere-egu24-20508.
- Wu, X., Ma, J., Si, X., Bi, Z., Yang, J., Gao, H., Xie, D., Guo, Z., Zhang, J., 2023. Sensing prior constraints in deep neural networks for solving exploration geophysical problems. Proceedings of the National Academy of Sciences 120, e2219573120. doi:10.1073/pnas.2219573120.
- Yu, S., Ma, J., 2021. Deep Learning for Geophysics: Current and Future Trends. Reviews of Geophysics 59, e2021RG000742. doi:10.1029/2021RG000742.